Jurnal Teknologi

Full paper

Simulative Study of Two-Phase Homogenous and Isotropic Media Imaging using Magnetic Induction Tomography

Zulkarnay Zakaria[a*], Ibrahim Balkhis[a], Lee Pick Yern[a], Nor Muzakkir Nor Ayob[b], Mohd Hafiz Fazalul Rahiman[a], Mohd Zikrillah Zawahirah[a], Ruzairi Abdul Rahim[b]

[a]*Tomographic Imaging Research Group, School of Mechatronic Engineering, Universiti Malaysia Perlis, 02600, Arau, Perlis, Malaysia*
[b]*Process Tomography and Instrumentation Engineering Research Group (PROTOM-i), Infocomm Research Alliance, Faculty of Electrical Engineering, Universiti Teknologi Malaysia, 81310 UTM Johor Bahru, Johor Malaysia*

Corresponding author: zulkarnay@unimap.edu.my

Article history

Received :7 February 2014
Received in revised form :
3 April 2014
Accepted :2 May 2014

Graphical abstract

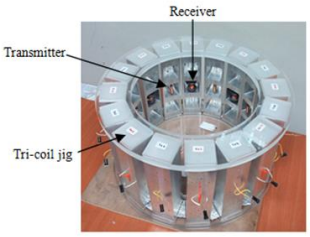

Abstract

Magnetic induction tomography is a new non-invasive technology, based on eddy current discovery of electromagnetic induction by Michael Faraday. Through this technique, the passive electrical properties distribution of an object can be obtained by the use of image reconstruction algorithm implemented in this system. There are many types of image reconstruction that have been developed for this modality, however in this paper only two algorithms discussed, Linear Back Projection and Eminent Pixel Reconstruction. Linear Back Projection algorithm is the most basic type of image reconstruction. It is the simplest and fast algorithm out of all types of algorithms, whereas Eminent Pixel Reconstruction algorithm is an improved algorithm which provided better images and has been implemented in other modalities such as optical tomography. This paper has implemented Eminent Pixel Reconstruction in magnetic induction tomography applications and the performance is compared to Linear Back Projection based on the simulation of the fourteen types of simulated phantoms of homogenous and isotropic conductivity property. It was found that Eminent Pixel Reconstruction has produced better images relative to Linear Back Projection, however the images are still poor when the objects are located near to the excitation coil or sensor and it is worse when the distance between objects are near to each other.

Keywords: Magnetic induction; tomography; image reconstruction algorithm; isotropic; low conductivity.

1.0 INTRODUCTION

Magnetic Induction Tomography (MIT) is a technique interested in passive electrical properties (PEPs) that are conductivity, permittivity and permeability. MIT attempts to image the PEPs distribution within an object space non-invasively. This modality is categorized as passive imaging family together with Electrical impedance tomography (EIT), Electrical Capacitance tomography (ECT) and Magnetostatic Permeability Tomography (MPT)[1,2]. The general principle on magnetic induction tomography is that coils are used to generate an oscillating magnetic field which induced eddy current in the object due to its conductivity. These eddy currents then generate secondary magnetic fields and will be measured by the sensors at the receiver[3,4]. Even though both primary signals and secondary signals exist at the sensors, only secondary signal is the interest of MIT modality as it carries the info on the electrical properties of the material which then transformed to an image.

In metal imaging where the conductivity is very high, secondary signals recorded by the sensors is not a big issue as the value is relatively higher which is up to 10^6 compared to low conductivity materials such as biological tissues[5]. In metal imaging especially in molten steel processes, real time scheme is the priority as monitoring the flow of molten steel during the process is crucial compared to high contrast issue. Thus the applied algorithm has to be fast enough to suit the requirement of the real time system and Linear Back Projection (LBP) is the best option to that[6].

In different to low conductivity imaging, especially in biomedical tissue, high contrast issue has become the priority compared to speed of the image generation. In human body, an organ is built by several tissues which located close to each other and comes with different properties. Thus when an health issue exist (i.e. tumor), a high resolution screening process is needed as the objective is to highlight the boundary of the tumor which may covers several part of the tissues. In achieving this, a more thorough study on the algorithm is crucial in solving the low resolution and inaccurate issues of the reconstructed images.

This paper discusses the weaknesses and limitations of the LBP algorithm in the MIT imaging system through simulation with several simulated phantoms of different sizes and shapes. The enhancement of the images quality through the use of EPR algorithm as an enhancement to the LBP also has been tested and compared. The info on the performances will be the additional inputs to the future research in finding the better solution to the

reconstructed images in term of resolution, shapes and size accuracy.

2.0 MIT MODEL AND SENSITIVITY MAPS

The developed MIT system of this research consisted of a TRI-COIL sensor jig design as in Figure 1, with 8 transmitter panels and 8 receiver panels which were arranged alternately at equidistance between each in circular way. Each panels had three 4cm×4cm×4cm dimension slots where each slot was located with transmitter in transmitter panels and so with the receivers. In total for all the three layers, there were 24 transmitters and 24 receivers with each layer consisted of 8 transmitters and 8 receivers. In this research, the simulation is only done on single layer (middle layer), since this paper wanted to analyze the performance of EPR and LBP algorithm at single layer basis on the developed MIT system. At single layer basis, each transmitter will undergo 8 projections which for 8 receivers in total produced 64 projections which then contribute to the sensitivity maps of the MIT system. Sensitivity map is a set of matrices of the projected path from one transmitter to one receiver of a system. Each pixel in the sensitivity map represents the sensitivity area of the wave propagation [7–9].

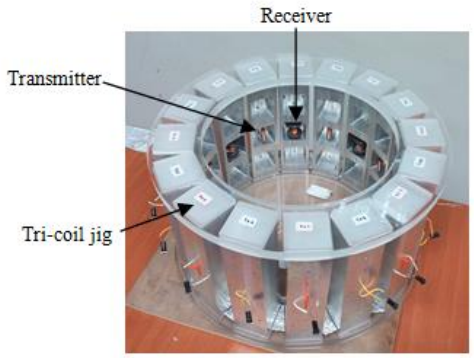

Figure 1 Tri-coil sensor jig with transmitter and receiver

3.0 IMAGE RECONSTRUCTION ALGORITHMS

There are many types of image reconstruction algorithms such as linear back projection, non-linear algorithm and filtered back projection, however in this project, LBP algorithm is used as a basis for comparison to EPR algorithm.

The LBP algorithm is based on matrix multiplication in such as it requires several multiplications to be performed. In order to reconstruct the image, each sensitivity matrix is multiplied by its corresponding sensor reading; where this is the same as back project each sensor reading to image plane individually. The mathematical equation for LBP is[10,11]:

$$V_{LBP}(x,y) = \sum_{Tx=0}^{8}\sum_{Rx=0}^{8} S_{Tx,Rx}\ X\ \bar{M}_{Tx,Rx}(x,y) \quad (1)$$

Where,
$V_{LBP}(x,y) =$ Voltage distribution obtained using LBP algorithm in n x n matrix where n is equals to dimension of sensitivity maps.
$S_{Tx,Rx}$ = Signal loss amplitude of receiver Rx-th for projection Tx-th in unit of volt.
$\bar{M}_{Tx,Rx}(x,y)$ = The normalized sensitivity matrices for the view of Tx-Rx.

Eminent Pixel Reconstruction (EPR) is an algorithm that is derived from the basic reconstruction algorithm of LBP. This new image reconstruction algorithm successfully highlights high intensity pixels from the surrounding pixels in the cross-section image. If the value equals to or less than the concentration threshold preset, the final values are set to zero. This is a threshold method which is by changing the pixel values depending on whether they are less or greater than the specified threshold. The following equations simply show the concept of EPR algorithm [9].

$$B(x,y) = \prod_{Rx}^{8}\prod_{Tx}^{8} Z_{Rx,Tx} \begin{cases} Z_{Rx,Tx} = 0; & S_{Rx,Tx} \le P_{Th} \\ Z_{Rx,Tx} = 1; & S_{Rx,Tx} > P_{Th} \end{cases} \quad (2)$$

$$V_{EPR}(x,y) = B(x,y) \times V_{LBP}(x,y) \quad (3)$$

Where,
$B(x,y)$ = EPR marking matrix, 1 represent eminent pixels.
$V_{LBP}(x,y)$= Reconstructed concentration profile using LBP algorithm
$V_{EPR}(x,y)$ = Improved concentration profile using ERP algorithm

Since biological tissue has been the interest in this research, it is important to touch a little bit on the algorithm similarity of CT-Scanner and Magnetic Resonance Imaging (MRI) as all involves in biological tissue imaging. In the first place, CT Scanners utilizing x-ray source in its imaging technique whereas MRI applied very high magnitude of magnetic field to align the hydrogen nuclei in the body. In these both modalities, LBP has been the basic of image reconstruction algorithm at their early development stage, but has progressed up to the current level which capable of producing a very high resolution reconstructed images. As a hard field modality, CT Scan still adopt LBP concept with some modification and hybridization and utilizes the attenuation of x-rays by biological tissues as signals for generating the images[12,13]. In different to MRI, nonlinear approach has been chosen it its current algorithm as magnetic field is nonlinear and ill posed nature, thus a nonlinear method is incapable of producing a very high contrast images between each tissues [14,15].

3.1 Composition of Pixels Concentration Profile

By computing the composition of the image pixel concentration, the performance of the image reconstruction algorithm can be determined. The composition determination is to extract more information of the reconstructed profile. In the reconstruction process, the reconstructed image's pixels are distributed according to different color profile.

Calculation of the concentration distribution for component *A* and *B* is as follows:

$$A = \frac{\sum_{y=1}^{64}\sum_{x=1}^{64} V(x,y)}{M_p} \times 100 \quad (4)$$

$$B = \left(1 - \frac{\sum_{y=1}^{64}\sum_{x=1}^{64} V(x,y)}{M_p}\right) \times 100 \quad (5)$$

Where;
A is the percentage of pixel concentration at threshold value and above.
B is the percentage of pixel concentration less than pixel threshold value.
V(x,y) is the obtained pixel values for 64 × 64 pixels concentration profile.
M_p are the maximum total pixel values, 32550.

3.2 Error Measurement of Image Reconstruction

Error measurement for image reconstruction in this project is by calculating the pixel concentration error of the reconstructed image. Calculation for pixel concentration error is the difference between the exact values and reconstructed values divide by the exact values. The result is then multiplied by 100 percentages to get a percentage value. The formula for pixel concentration error measurement is as follows:

$$\% \text{ Pixel concentration error} = \frac{Exact - Reconstructed}{Exact} \times 100 \quad (6)$$

Where, *Exact* is the true pixels concentration of the phantom in SimMap before undergoing any reconstruction process, whereas *Reconstructed* is the pixel concentration of the phantom after reconstruction process.

The pixel concentration area of the phantom is computed as the summation of the maximum pixel values for the phantom. It can be easily computed by using the formula in (6) and is represented in mm² unit. For easy computation, composition *B* is used for the pixel concentration area computation instead of composition *A*. Composition *B* is totally the 0 pixel values which are represented by blue color. Composition *A* is a matrix consists of a set of variable of the pixel values bigger than 0 other than blue color. Therefore, it is hard to compute only the maximum threshold values since during the reconstruction some noises which are unwanted pixels are still present. There is still some affected area around the desired phantom represented by green, yellow and cyan color due to the algorithm inefficiency and limited accuracy.

4.0 RESULTS AND DISCUSSION

The simulation in obtaining the images has been developed based on MATLAB version R2010 software. The phantom created in this simulation is the homogeneous phantom which contains a set of binary matrices. There is only 2 dimensional (2D) phantom has been carried out. The shape of the biological tissues is not exactly same as the real tissues but is replaced by the square and round shape that is mimicking the biological tissues. Figure 2 shows the types of phantom that has been created and Figure 3 display the reconstructed images of phantom (*f*) using LBP and EPR algorithm. SimMap is referring to the phantom before undergoing any image reconstruction and *A* is any pixel values other than zero whereas *B* is referred to zero pixel value represented by the deep blue color.

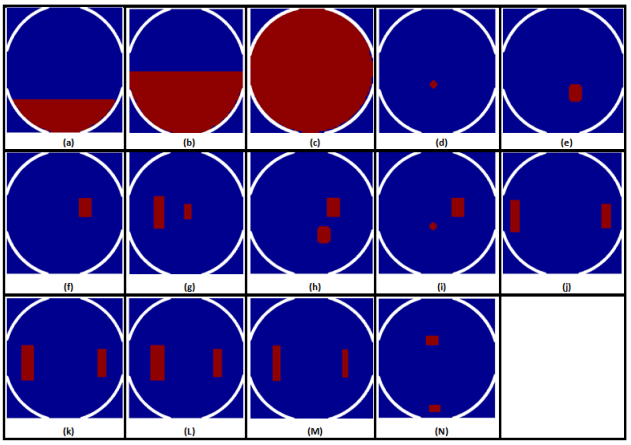

Figure 2 Types of phantoms with different position

Map/Reconstruction method	Phantom	Reconstructed Image	Concentration Distribution (%)		Area (mm²)	
			A	B	A	B
SimMap	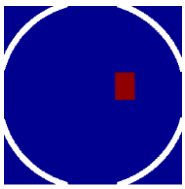	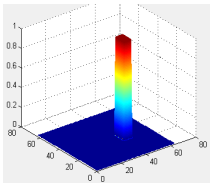	0.22	99.78	71.61	32478. 39
LBP	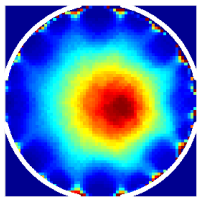	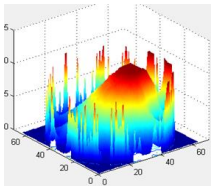	41. 07	58. 93	13374.80	19175.21
EPR Threshold ≈ 10	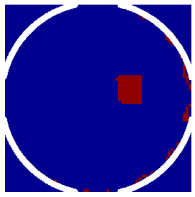	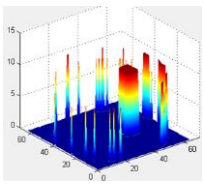	4.06	95.9	1321.53	31228.47

Figure 3 Reconstructed images of phantom (*f*) using LBP and EPR

Figure 4 shows the reconstructed images of phantom *(d), (g), (i)* and *(j)* using EPR algorithm at different threshold values. By increasing the intensity, the image is better in term of quality and has least percentage of error measurement. However, even increasing the intensity value to the optimum, there are still some errors in the images due to very high sensitivity near the sensors. On the other hand, the EPR algorithm also cannot solve the problem for the very close distance of phantoms, hence produce a single image even for a dual close objects. Some improvement of this algorithm is still needed in solving this problem.

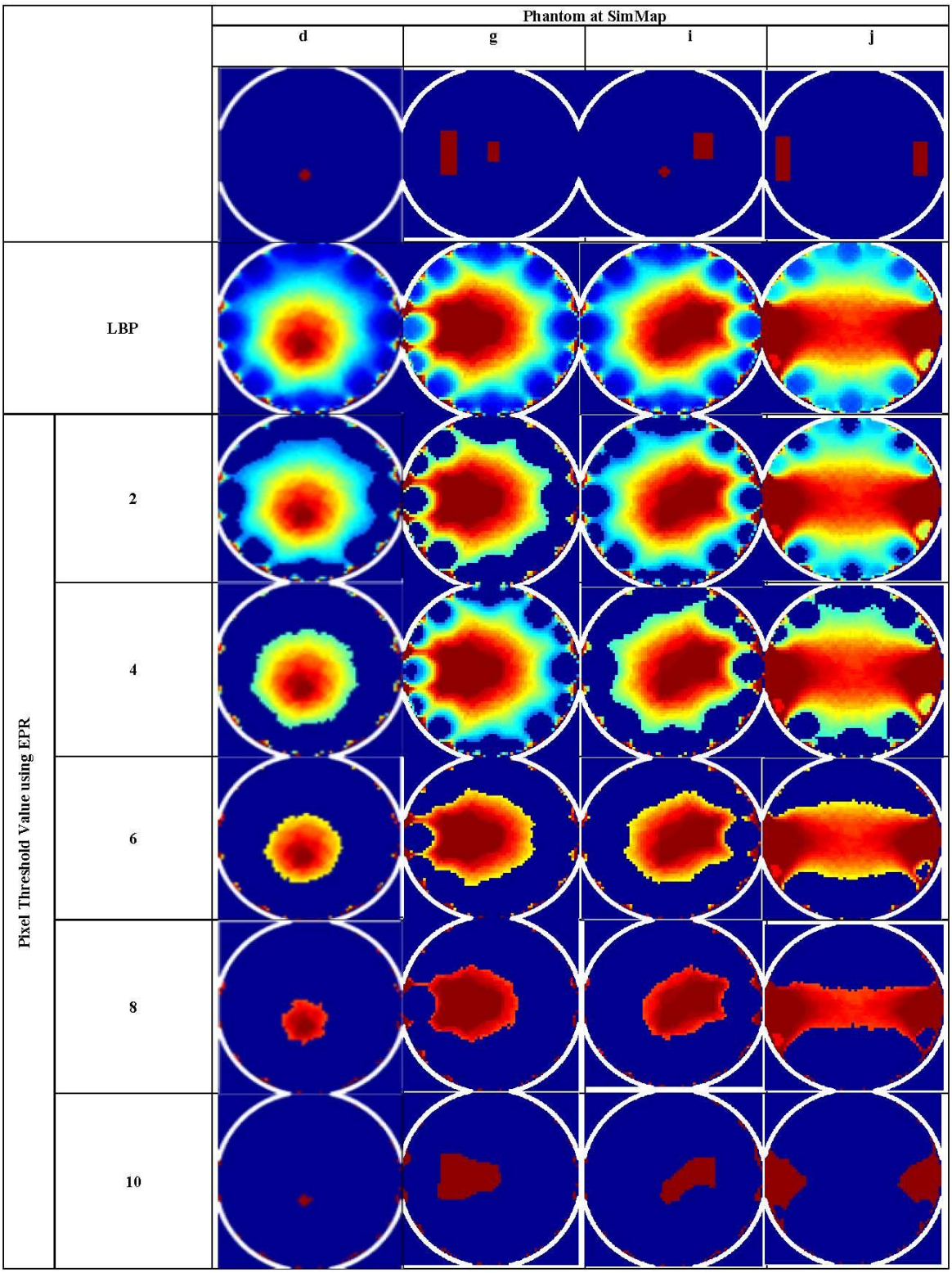

Figure 4 Reconstructed images of phantom *(d), (g), (i) and (j)* using EPR at different pixel threshold value

The graph in Figure 5 show the comparison between pixel concentration and error measurement for a selected phantom whereas Figure 6 displays the performance comparison of EPR and LBP algorithm on the reconstructed images in MIT.

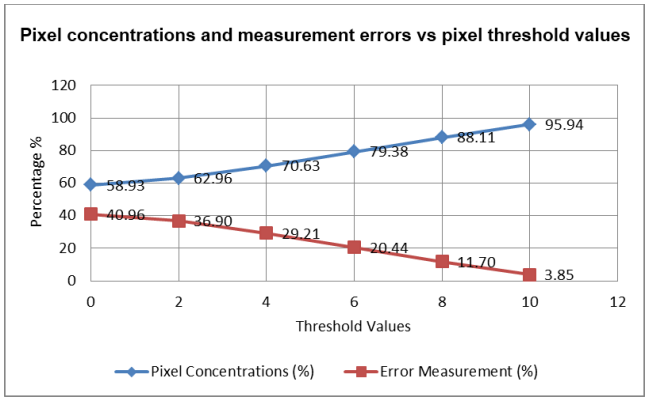

Figure 5 Graph of pixel concentration and error measurement vs. different threshold values for phantom *(e)*

The measurement error is based on the calculation of the area of phantom in two phases which is before and after undergoing reconstruction in percentage. Figure 6 shows the area error for 14 different types of phantom based on LBP and EPR algorithm.

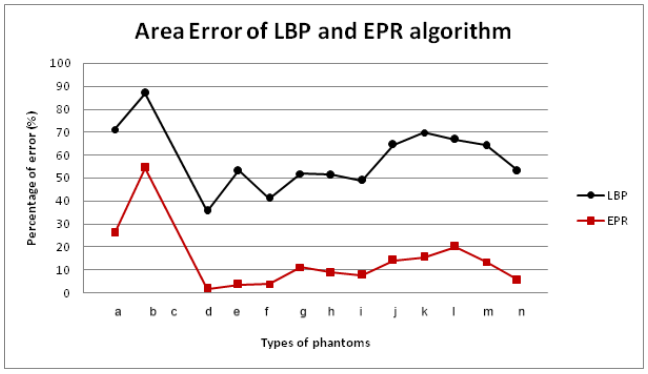

Figure 6 The area error measurement of LBP and EPR for all 14 types of phantoms

Based on the results, the percentage of error measurement for LBP is higher than EPR for all types of phantoms and approximately up to 30% compared to EPR. Images reconstructed using LBP are accompanied by noises due to smearing effect exist in this algorithm, whereas EPR algorithm filtered this effects at a certain degree of adjusted intensity values from 1-10 and highlights high density values in respective to the background. From the above results, it is clearly shown that EPR is much more efficient and provided higher accuracy compared to LBP. By varying the intensity values, the image accuracy is also varied, but the quality of the reconstructed images still at low resolution level. It is clear that, even EPR has been implemented there are still high intensity points at the internal side of the boundary of region of interest (ROI) due to the excitation coils located at the position. At these points, higher magnitude of magnetic fields is generated and had contributed errors to the reconstructed images.

5.0 CONCLUSIONS

MIT modality provides opportunity in non-invasive, non-intrusive and to date as far as the authors are concern, there is no reported radiation effects on this technique. However due to the existing of the so called ill-posed problem in this passive imaging modality, LBP and EPR image reconstruction algorithm do not have enough capability in producing quality reconstructed images of the objects because linear methods cannot solve the behavior of the nonlinear pattern. However, these two algorithms provided informative info on the constraints and limitations faced by MIT modality such as resolution and shape of the object together with the minimal distance of each object itself. Enhancements need to be done in the algorithm in such that higher accuracy image is vital if MIT wants to be applied in the medical tissue imaging or in high speed movement of liquid material in a pipeline. As magnetic field is nonlinear and ill-posed in nature, thus nonlinear algorithm is the best solution in providing the best solution to the above mentioned issues. On the other hand, processing time issue as a drawback to the iteration from such algorithm has to be put into consideration when discussing the nonlinear technique.

Acknowledgement

The authors would like to thank the Universiti Malaysia Perlis, Universiti Teknologi Malaysia and Ministry of Science Technology and Innovation for supporting this research. This work is supported by UTM under Vot R.J130000.7813.4F254.

References

[1] Soleimani, M. 2008. Computational Aspects of Low Frequency Electrical and Electromagnetic Tomography: A Review Study. *International Journal of Numerical Analysis and Modelling*. 5: 407–440
[2] Zakaria, Z., Rahim, R.A., Mansor, M.S.B.,Yaacob, S., Ayob, N. M. N., Muji, S.Z.M., Rahiman, M.H.F. and Aman, S. M. K. S. 2012. Advancements in Transmitters and Sensors for Biological Tissue Imaging in Magnetic Induction Tomography. *Sensors*. 12: 7126–7156
[3] Tian, G. Y., Al-Qubaa, A. & Wilson, J. 2012. Design of an Electromagnetic Imaging System for Weapon Detection Based on GMR Sensor Arrays. *Sensors and Actuators A: Physical*. 174: 75–84.
[4] Griffiths, H. 2001. Magnetic Induction Tomography. *Measurement Science and Technology*. 12: 1126–1131.
[5] Griffiths, H. 2005. Magnetic Induction Tomography. *Electrical Impedance Tomography: Methods, History and Applications*. 213–238
[6] Terzija, N., Yin, W., Gerbeth, G., Stefani, F., Timmel, K., Wondrak, T., Peyton, A. J. 2011. Use of Electromagnetic Induction Tomography for Monitoring Liquid Metal/Gas Flow Regimes on a Model of an Industrial Steel Caster. *Measurement Science and Technology*. 22: 1–8.
[7] Nor Ayob, N. M., Zakaria, Z., Fazalul Rahiman, M. H., Abdul Rahim, R. & Yaacob, S. 2011. Initial Development on Magnetic Induction Tomography Imaging. *Jurnal Teknologi*. 55: 11–14.
[8] Soleimani, M. 2006. Sensitivity Maps in Three-dimensional Magnetic Induction Tomography. *Insight-Non-Destructive Testing and Condition Monitoring*. 48: 39–44.
[9] Yin, W. & Peyton, A. J. 2010. Sensitivity Formulation Including Velocity Effects for Electromagnetic Induction System. *IEEE Transactions on Magnetics*. 46: 1172–1176.
[10] Fazalul Rahiman, M. H., Abdul Rahim, R. & Zakaria, Z. 2008. Design and Modelling of Ultrasonic Tomography for Two-component High-acoustic Impedance Mixture. *Sensors and Actuators A: Physical*. 147: 409–414.
[11] Nor Ayob, N. M., Fazalul Rahiman, M. H., Zakaria, Z., Abdul Rahim, R. & Yaacob, S. 2011. Eminent Pixel Reconstruction Algorithm For Ultrasonic Tomography. *Jurnal Teknologi*. 55: 15–22.

[12] Ritman, E. L. 2004. Micro-computed Tomography-current Status and Developments. *Annual Review of Biomedical Engineering*. 6: 185–208.
[13] Haff, R. P. & Toyofuku. 2008. N. X-ray detection of defects and contaminants in the food industry. *Sensing and Instrumentation for Food Quality and Safety*. 2: 262–273.
[14] Gore, J. C., Manning, H. C., Quarles, C. C., Waddell, K. W. & Yankeelov, T. E. 2011. Magnetic Resonance in the Era of Molecular Imaging of Cancer. *Magnetic Resonance Imaging*. 29: 587–600.
[15] Thybo, A. K., Jespersen, S. N., Laerke, P. E. & Stødkilde-Jørgensen, H. J. 2004. Nondestructive Detection of Internal Bruise and Spraing Disease Symptoms in Potatoes Using Magnetic Resonance Imaging. *Magnetic Resonance Imaging*. 22: 1311–7.